Deep ultraviolet hyperspectral cryomicroscopy in boron nitride: Photoluminescence in crystals with an ultra-low defect density

Pierre Valvin, Thomas Pelini, Guillaume Cassabois, Alberto Zobelli, Jiahan Li, J. Edgar, Bernard Gil

AIP Advances

Deep ultraviolet hyperspectral cryomicroscopy in boron nitride: Photoluminescence in crystals with an ultra-low defect density

Cite as: AIP Advances **10**, 075025 (2020); https://doi.org/10.1063/5.0013121
Submitted: 09 May 2020 . Accepted: 05 July 2020 . Published Online: 28 July 2020

Pierre Valvin, Thomas Pelini, Guillaume Cassabois, Alberto Zobelli, Jiahan Li, James H. Edgar, and Bernard Gil

Deep ultraviolet hyperspectral cryomicroscopy in boron nitride: Photoluminescence in crystals with an ultra-low defect density

Cite as: AIP Advances 10, 075025 (2020); doi: 10.1063/5.0013121
Submitted: 9 May 2020 • Accepted: 5 July 2020 •
Published Online: 28 July 2020

Pierre Valvin,[1] Thomas Pelini,[1,2] Guillaume Cassabois,[1] Alberto Zobelli,[3] Jiahan Li,[4] James H. Edgar,[4] and Bernard Gil[1,a)]

AFFILIATIONS

[1]Laboratoire Charles Coulomb, Université de Montpellier, Case Courrier 074, 34095 Montpellier Cedex 5, France
[2]LNCMI-CNRS, B.P. 166, 25, Rue des Martyrs, 38042 Grenoble, France
[3]Université Paris-Saclay, CNRS, Laboratoire de Physiques des Solides, 91405 Orsay, France
[4]Tim Taylor Department of Chemical Engineering, Kansas State University, Manhattan, Kansas 66506, USA

[a)]**Author to whom correspondence should be addressed:** bernard.gil@umontpellier.fr

ABSTRACT

We report the development of a scanning confocal microscope dedicated to photoluminescence in the 200 nm-wavelength range for samples at cryogenic temperatures (5 K–300 K). We demonstrate the performances of our deep ultraviolet cryomicroscope in high-quality hexagonal boron nitride (hBN) crystals, although it can be utilized for biological studies in its range of operating wavelengths. From the mapping of photoluminescence, we bring evidence for the suppression of extrinsic recombination channels in regions free from defects. The observation of emission spectra dominated by intrinsic recombination processes was never reported before in hBN by means of photoluminescence spectroscopy. We show that photoluminescence tomography now competes with cathodoluminescence and that deep ultraviolet cryomicroscopy by photoluminescence is a novel powerful tool in materials science applications, with the great advantage of an efficient non-invasive photo-excitation of carriers.

Hexagonal boron nitride (hBN) is the wide-bandgap semiconductor that is currently booming, as it interfaces the worlds of 2D-materials and wurtzitic semiconductors. Researchers working on 2D materials use it abundantly as a barrier material for passivating the surfaces in van der Waals heterostructures.[1,2] Researchers working on nitride semiconductors now positively consider hBN as an alternative to GaN–AlN alloys for deep ultraviolet (DUV) emission. While GaN–AlN saturates to wavelengths longer than 235 nm,[3] hBN lasing action at 215 nm in cathodoluminescence (CL) experiments was demonstrated as early as 2004 by Watanabe and Taniguchi.[4] They reported an intense light emission in the DUV for this semiconductor soon after they grew hBN crystals having millimeter sizes.

DUV emission is of paramount importance for biological applications. Wavelengths in the 260 nm–270 nm range are strongly absorbed by DNA.[5] Regions of shorter wavelengths are also interesting, and hBN-based emitters will be strategic devices for sterilization by destructing nucleic acids (DNA and RNA) by fully covering the 200 nm–300 nm wavelength range. Below 220 nm, the germicidal efficiency relies on UV absorbance due to the transitions of the planar purine and pyrimidine bases.[6] However, the detailed analysis of light–matter interaction for DNA in the 200 nm range when the system is photo-perturbed (for instance, under a dense photo-excitation) is in its infancy. A bright future is expected for hBN-based light emitters used as efficient DNA breakers to directly kill viruses such as, for example, SARS-CoV-2, and to jeopardize the existence of bacteria propagating nosocomial diseases. The spatial resolution of our device makes it rather useful for tomographic probings inside genuine cells or in cells with specific localized biological modifications.

A variety of other applications have been suggested for hBN. In 2012, Jiang and his group at the Texas Tech University reported hBN-AlGaN *pn* junctions, and they proposed a design for hBN-based light emitting diodes (LEDs).[7] Makimoto *et al.*[8] and Kobayashi *et al.*,[9] almost at the same time, demonstrated that the lamellar structure of hBN can serve as a sacrificial layer deposited at the interface between the active part of a nitride-based LED and its expensive substrate, making it possible to reuse the latter and, by doing so, to decrease the cost of the device. hBN also contains several defects that can be used as super bright single photon sources (SPSs) operating from 1.8 eV (~700 nm) up to 4 eV (~300 nm).[10–12] In summary, hBN is an ultra-wide bandgap semiconductor with promising optoelectronic properties in the DUV, which motivated the construction of a scanning confocal microscope dedicated to PL experiments down to a wavelength of 200 nm for samples at cryogenic temperatures.

We now present of our unique setup, followed by the discussion of its performances. More specifically, we present spatially resolved PL measurements in the DUV showing strong variations in the defect-related emission in bulk hBN samples. We isolate hBN monocrystals with an almost complete suppression of extrinsic recombination channels. Our results demonstrate that our DUV cryomicroscope competes with the CL technique for detailed characterization in materials science, with the intrinsic advantage of the PL technique that relies on an efficient non-invasive generation of carriers in the samples.

Recent studies have reported spatially resolved optical studies in the DUV. Watanabe and Taniguchi reported a PL microscope that is restricted to room-temperature measurements.[13] Its excitation is based on an incoherent light source provided by a spectrally filtered deuterium lamp, thus leading to a poor spatial resolution of the PL experiments. Ishii *et al.*[14] proposed a solution relying on near-field measurements. The latter DUV scanning near-field optical microscope (SNOM) reaches a spatial resolution down to 150 nm, but with the usual drawback of the SNOM technique that it is limited to low fluxes of the emitted photons.

We developed a DUV far-field microscope with two major improvements: (i) a spatial resolution down to the diffraction limit by using a coherent laser excitation and (ii) an operation at cryogenic temperatures for an in-depth investigation of fundamental optoelectronic processes. Combining both aspects is a real challenge in the DUV spectral domain. Because of the strong chromatic aberrations in the DUV, reflective optics are mandatory. Still, a crucial point is the positioning of the microscope objective inside the vacuum chamber of the cryostat in order to avoid the aberrations induced by the optical windows of the cryostat. The design of the microscope was controlled and optimized using the commercial software Zemax®.[15] Figure 1 presents an opto-mechanical sketch of our instrument.

The excitation is provided by the fourth harmonic of a cw mode-locked Ti:Sa oscillator (Chameleon-Coherent©), which is tunable between 193 nm and 205 nm. Note that atmospheric dioxygen absorption occurs at wavelengths below 196 nm so that the related Shumann–Runge absorption bands may affect the laser power. The laser beam is spatially filtered in a 10 μm pinhole before injection into the microscope. The best option for the injection would have been a dichroic mirror at a 45°-incidence angle with a sharp cutoff at 205 nm. Since such a dichroic mirror is not available, the laser is injected through a double reflection system with a pair of dichroic mirrors at 22.5° provided by Layertech©. After filtering and routing, the maximum laser power is 1 mW at 196 nm at the sample surface.

The critical points of the setup design deal with the management of the issues related to optics in the UV spectral domain, i.e., the strong variations in the complex refractive index that lead to chromatic aberrations, on the one hand, and to absorption by the optical components, on the other hand. These issues become more and more stringent when working deeper and deeper in the UV, restricting the choice of the relevant optical parts to be used for DUV cryomicroscopy. A straightforward way to suppress chromatic aberrations consists in replacing refractive optics by the reflective ones. Nevertheless, the low-temperature operation of our setup makes unavoidable the refraction through the optical window of the cryostat, which can dramatically degrade the performances of the cryomicroscope. Our simulations indicate that the spot of our DUV laser at ~200 nm is diffraction-limited without refraction through a glass plate and that its size increases to 20 μm if a 0.5 mm-glass plate is introduced in the optical path between the microscope and the sample. As a consequence, the reflective microscope objective has to be integrated inside the cryostat. This imposes a large vacuum chamber. Our cryostat is a custom closed-cycled design system from MyCryoFirm©, allowing long-term experimental runs. The lowest temperature of the sample holder is ~5 K, and the amplitude of the

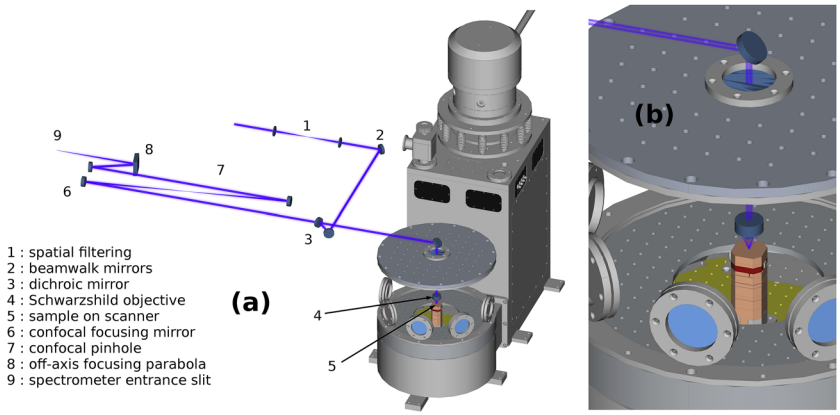

FIG. 1. Principle of the μPL experimental setup. (a) Sketch of the whole optical setup. (b) Zoomed-in view of the cryostat.

mechanical vibrations is below 15 nm rms. In order to map the PL signal at different positions of the sample, we use piezoelectric XYZ scanners from Attocube© on top of large range XYZ nanopositioners. We use a reflective objective with a numerical aperture (NA) of 0.5 commercialized by Thorlabs©, compatible with vacuum operation. We obtain a laser spot with a size of ~300 nm close to the theoretical diffraction-limited value ($\lambda/2NA \sim 200$ nm).

All the optics in the detection path are reflective. For confocal filtering, spherical mirrors are used with an off-axis angle limited to 8° in order to keep a diffraction-limited spot on the confocal pinhole. For imaging on the spectrometer entrance slit, we chose an off-axis parabolic mirror. All mirrors are made of aluminum, protected with a MgF_2 coating. For the detection and analysis of the DUV luminescence, we use a Czerny–Turner spectrometer from Andor©. The focal length is 500 mm, and the DUV grating is holographic with 1800 grooves/mm. The camera is a back-illuminated Andor/Newton940 CCD with BIU2 AR-coating, where the pixel size is 13.5 μm. The sensor quantum efficiency is 35% at 200 nm and 60% at 300 nm, with a maximum of 68% at 250 nm. The spectral resolution $\Delta\lambda$ is measured with the 205.28 nm radiation of an Hg spectral source. We estimate $\Delta\lambda = 0.04$ nm (1.3 meV). In the following, we present measurements in high-quality hBN crystals using our scanning confocal DUV cryomicroscope for spatially resolved PL experiments.

High-quality hBN crystals, ^{11}B monoisotopic, were grown by precipitation via the metal flux method.[15–17] The molten metal solution was first saturated with boron and nitrogen at a high temperature, 1550 °C; then, by slowly cooling the solution, boron and nitrogen solubility decreased, leading to the formation of h^{11}BN crystals. In this case, the metal was high-purity, low carbon (1 ppm) iron, the high purity boron source was 99.41 at. % ^{11}B, and nitrogen originated from the gas flowing over the solution. A description of the experimental setup is given in Ref. 17. Figure 2 shows the photograph of our hBN sample that was detached from the metallic ingot used to grow it by reversed solidification at the Kansas State University.[16] This image was taken using a Leica DVM6 digital optical microscope. The thickness of the hBN crystal in this image varied between 10 and 20 μm.

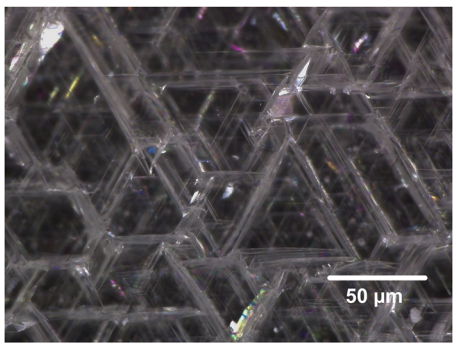

FIG. 2. Surface of a hBN crystal with characteristic steps, typical of the growth procedure used at KSU. This image was taken using a Leica DVM6 digital optical microscope. The thickness of the hBN crystal in this image varied between 10 and 20 μm.

One distinguishes linear extended defects defining complete or truncated hexagons. These defects derive from the specific honeycomb lattice of hBN, and it was demonstrated by CL measurements that these defects play a key role in the extrinsic luminescence signal at energies below 5.6 eV.[19] Thanks to the high value of the absorption coefficient of BN we measured on this sample, which is about 4×10^{-5} cm^{-1} in the range between 195 nm and 190 nm, the photons of the laser beam penetrating in the sample are all absorbed.

Before presenting our results using our DUV cryomicroscope, we highlight that there is no emission around 4.1 eV in these hBN crystals, in contrast to prior studies.[19] Since the spectral domain around 4.1 eV is ubiquitous for the emission of deep levels, this observation witnesses the exceptional purity of the samples under examination.

Figure 3(a) is a representative PL spectrum recorded at a low temperature. The luminescence signal in the 5.90 eV–5.75 eV range (200 nm–215 nm) is of intrinsic nature. It corresponds to the phonon-assisted recombination of the indirect exciton (ix) involving phonons at the T_1 point of the Brillouin zone (BZ).[19] The fundamental bandgap of BN is indirect in reciprocal space, with the minimum of the conduction band at **M** and the maximum of the valence band near K. The phonon involved in the first phonon recombination process should have a wave vector KM, which is, thanks to a group theory argument, equivalent to a phonon at T_1, that is, at the center of the BZ, along the Γ**K** direction. In our notation, we use the convention of Ref. 19 where ix means indirect exciton. The sharp phonon-assisted transitions form a series of lines related to (from high to lower energy) the TA, LA, TO, and LO phonon modes giving rise to emission at 5.89 eV, 5.86 eV, 5.79 eV, and 5.76 eV, respectively. Note that the TO-assisted recombination line is the sharpest of the series because of the low value of the group velocity of the TO phonon at the T_1 point of the BZ.[20] In Fig. 3(a), the sharp TO-line at 5.79 eV has a full width at half maximum of ~4.8 meV, attesting of the high quality of our hBN crystals and of the high performances of our setup. The phonon replicas further display a fine structure at their low energy side, with a prominent doublet, which is due to complementary inelastic Raman scattering involving the low frequency E_{2g} vibration mode.[21] Below 5.6 eV (220 nm), the luminescence signal is of extrinsic nature. Figure 3(a) shows the first emission spectrum recorded by PL spectroscopy in hBN where the intrinsic emission above 5.7 eV is more intense than the extrinsic emission below 5.6 eV, a feature previously only observed in CL measurements.

The defect-related emission below 5.6 eV is related to overtones of the intrinsic phonon-assisted emission, and these overtones involve (in addition to the primary phonon at the T_1 point) valley phonons at the K point of the BZ of hBN.[22] In Fig. 3(a), at 5.561 eV and 5.612 eV, we observe weak transitions, previously attributed to unknown impurities as the PL intensity does not follow the behavior of phonon assisted lines when increasing the temperature (feature at 5.5561 eV) and one-phonon 1TO(K) overtone (5.61 eV). The peaks at 5.461 eV and 5.490 eV are two-phonon 2TO(K) overtones. They are better resolved than by macro-PL, and the intensity of the two-phonon overtone is comparable to the intensity of the one-phonon overtone, which is a new result and again reinforces the interpretation of Refs. 20–22. We refer the readers to Refs. 19 and 20 for a correlation with the band-structure of BN for ix and for the phonon-assisted transitions. Regarding defects, they are not fully identified to

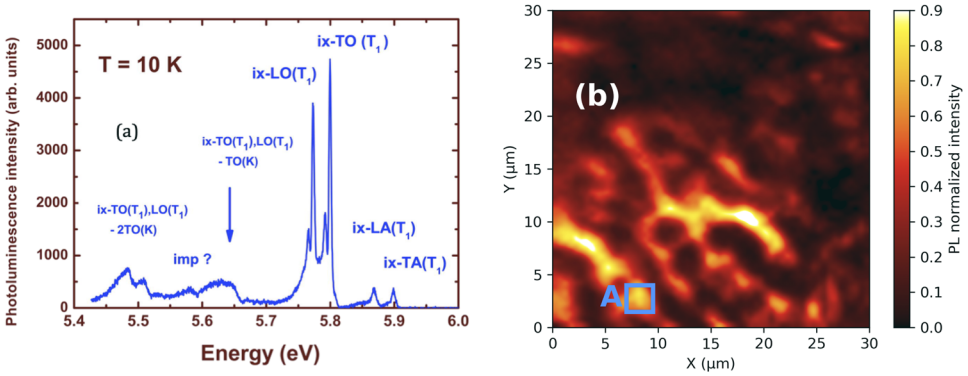

FIG. 3. (a) Low temperature PL spectrum recorded in a hBN monocrystal with ultra-low defect density. The defect-related PL signal (below 5.65 eV) is lower in intensity than the intrinsic-phonon-assisted transitions above 5.7 eV. (b) Tomography of the low temperature PL emission in the 5.72 eV–5.8 eV energy range in a 30 × 30 μm^2 region. A blue square noted A indicates the integrated area corresponding to panel (a).

date. When this will be achieved, theoretical calculations, when any, will teach us in terms of which weight their wave functions probe the different states of the BZ. We have plotted in Fig. 3(b) the spatial variations of the PL signal intensity in the 213.6 nm–216.6 nm (5.8 eV–5.72 eV) range, recorded in a 30 × 30 μm^2 region. A striking point is that our spatially resolved PL measurements reveal inhomogeneities of the intrinsic recombination signal. Hotspots and dark regions are observed with a size down to ~500 nm. The spatial distribution observed in Fig. 3(b) differs from the homogeneous one reported by CL measurements in thin hBN samples exfoliated from crystals synthesized at NIMS-Tsukuba.[23] Our results indicate that the relaxation dynamics display distinct phenomenologies in hBN crystals synthesized by various growth methods. Despite the high purity of our hBN crystals attested by the absence of any PL signal around 4.1 eV, clearly there is a striking inhomogeneous distribution of non-radiative recombination centers never reported before in PL.

Figure 4 shows the variations in the PL spectrum at different positions inside the 30 × 30 μm^2 region of Fig. 3. The PL spectrum recorded at position A in Fig. 4(b) is plotted in blue in Fig. 4(a) . It displays three broad PL bands at 5.62 eV, 5.55 eV, and 5.47 eV. We hardly observe the near band-edge phonon-assisted intrinsic recombination above 5.7 eV (not visible in the linear plot of Fig. 4). This spectrum is recorded at a position corresponding to a hotspot in the PL intensity map integrated in the 5.52 eV–5.59 eV energy range. Similarly to Ref. 18, the comparison of Figs. 3(b) and 4(b) shows a spatial anti-correlation of the PL intensity distributions depending on the intrinsic or extrinsic origin of the PL signal. The PL spectrum recorded at position B in Fig. 4(b) is plotted in green in Fig. 4(a). Its intensity has been magnified by a factor of 5. The fine structure of the broadbands is clearly resolved in the spectrum (gray line) recorded at position C, as a complementary evidence of the doublet nature of the PL bands at these energies. There is also a well-resolved doublet at 5.572 eV at the low energy side of a weak at 5.587 eV that was present at the low energy side of the composite PL of Fig. 3(a) that here peaks at 5.62 eV.

From Figs. 3 and 4 we conclude that our cryomicroscope for DUV PL spectroscopy has excellent spectral and spatial resolutions, enabling the resolution of inhomogeneities in high-quality hBN crystals and bringing important information for further improving the purity and quality of hBN in materials science.

Our DUV cryomicroscope for PL spectroscopy is a very powerful tool, complementing CL experiments that are widely used for the spectroscopy of wide bandgap semiconductors. Although the size of the electron beam in CL is much lower than the laser spot size in PL, carrier diffusion limits the effective spatial resolution in CL, of order 80 nm. This value is only four times smaller than our 300 nm-resolution, showing the very good spatial resolution of our PL setup. As far as the excitation itself is concerned, the photo-generation of carriers in PL is usually performed close to the bandgap, while CL relies on the absorption of electrons with an energy roughly three orders of magnitude higher than the incident photon energy in PL.

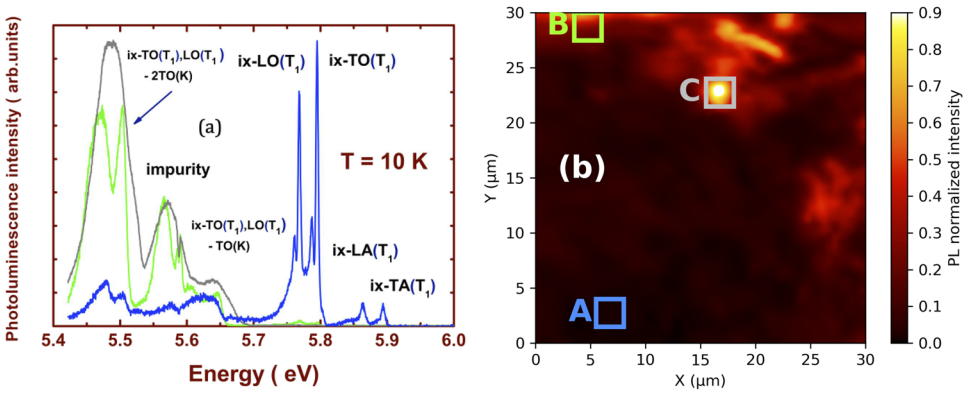

FIG. 4. (a) Photoluminescence spectra recorded in the three regions indicated in panel (b). The defect-related emission bands exhibit a doublet structure, whose contrast depends on the spectral width of the bands. (b) Tomography of the low temperature PL emission in the 5.52 eV–5.59 eV energy range in the same 30 × 30 μm^2 region as in Fig. 3(b). Note the anti-correlation with Fig. 3(b). (A) Blue spectrum, (B) green spectrum, and (C) gray spectrum in panel (a).

Such a high energy in CL may modify or perturb the atomic arrangement or the sample properties, while PL relies on the hardly invasive absorption of low-energy photons. Furthermore, laser excitation is superior for measuring the emission of hBN monolayers and characterizing the direct bandgap crossover in the monolayer limit.[24] In contrast, CL has been limited so far to the measurements of hBN samples thicker than six monolayers.[25] Boron nitride, as most of the layered materials and unlike more common semiconductors, is highly sensitive to high energy electron irradiation, and atom sputtering occurs mainly due to the direct collision between relativistic electrons and atomic nuclei. In perfect h-BN, the electron energy beam threshold for atom displacement is about 80 keV, but this value is strongly lowered for atoms neighboring atomic defects.[26–28] The observation by transmission electron microscopy of point defects and the growth of more extended defective structures have been reported many times in the literature.[29–31] State-of-the-art nanometric resolved cathodoluminescence is currently performed in a scanning transmission electron microscope operating in the 40 keV–100 keV energy range. By using limited acceleration voltages, a stable luminescence can then be recorded in perfect h-BN samples or samples involving extended defects.[18] However, the observation of emissions related to point defects is much more challenging due to their higher sensitivity to electron irradiation, which lead to blinking or bleaching effects[32] or to the appearance of broad emission lines.[11]

In standard cathodoluminescence within a scanning electron microscope (SEM), if the sample is thick, the incoming electron undergoes a series of elastic and inelastic collisions until all its energy is released, whereas the original electron probe size can be rather small, in the nanometer scale, the luminescent signal arises from this extended excitation volume that ultimately defines the achievable space resolution. These traditional limitations can be overcome by operating in a scanning transmission electron microscope (nano-CL). The use of a high voltage, on the one hand, allows us to produce a probe that could be arbitrary small and, on the other hand, strongly reduce the interaction between the beam and the sample. The broadening ("excitation pear") of the electron probe essentially vanishes in thin samples. It has been possible, for instance, to achieve a space resolution as low as few nanometers for individual quantum wells.[33,34] The ultimate resolution achievable in this nano-CL approach is then limited solely by the excitation diffusion lengths.[35]

In conclusion, we have reported the development of a DUV cryomicroscope for PL spectroscopy with wavelengths as short as 200 nm. We have applied our original technique to the characterization of high-quality hBN crystals. Our DUV cryomicroscope has allowed us to measure the first emission spectrum ever recorded by PL spectroscopy in hBN, where the intrinsic emission above 5.7 eV is more intense than the extrinsic emission below 5.6 eV, a feature previously only observed in CL measurements. Despite the high purity of our hBN crystals attested by the absence of any PL signal around 4.1 eV, our spatially resolved PL measurements evidence a striking inhomogeneous distribution of the intrinsic PL signal, which we interpret as being related to non-radiative recombination centers. The physics of defects in hBN and the physics of its doping with foreign atoms are in their infancy. Complementary investigations are required for better understanding. We highlight the potentialities of our DUV cryomicroscope for PL spectroscopy in materials science, with the great advantage of allowing an optical characterization by the efficient non-invasive photo-excitation of carriers in PL spectroscopy.

AUTHORS' CONTRIBUTIONS

All authors contributed equally to this work.

We gratefully acknowledge Christian L'Henoret for his technical support at the mechanics workshop and Alrik Durand for his help in coding the data processing. P.V. acknowledges illuminating discussions with Ryota Ishii. This work was financially supported in France by the contract BONASPES (Grant No. ANR-19-CE30-0007) under the umbrella of the publicly funded Investissements d'Avenir program managed by the French ANR agency. T.P. acknowledges the financial support from the network GaNeX (Grant No. ANR-11-LABX-0014) for his Ph.D. GaNeX belongs to the publicly funded Investissements d'Avenir program managed by the French ANR agency. Support for hBN crystal growth from the National Science Foundation (Award No. CMMI 1538127) and the II–VI Foundation is greatly appreciated.

DATA AVAILABILITY

The data that support the findings of this study are available from the corresponding author upon reasonable request.

REFERENCES

[1] A. K. Geim and I. V. Grigorieva, "Van der Waals heterostructures," Nature **499**, 419–425 (2013).
[2] A. C. Gomez, "Why all the fuss about 2D semiconductors?," Nat. Photonics **10**, 202–204 (2016).
[3] A. A. Toropov, E. A. Evropeitsev, M. O. Nestoklon, D. S. Smirnov, T. V. Shubina, V. Kh. Kaibyshev, G. V. Budkin, V. N. Jmerik, D. V. Nechaev, S. Rouvimov, S. V. Ivanov, and B. Gil, "Strongly confined excitons in GaN/AlN nanostructures with atomically thin GaN layers for efficient light emission in deep-ultraviolet," Nano Lett. **20**, 158–165 (2020).
[4] K. Watanabe, T. Taniguchi, and H. Kanda, "Direct-bandgap properties and evidence for ultraviolet lasing of hexagonal boron nitride single crystal," Nat. Mater. **3**, 404–409 (2004).
[5] M. Kneissl, T.-Y. Seong, J. Han, and H. Amano, "The emergence and prospects of deep-ultraviolet light-emitting diode technologies," Nat. Photonics **13**, 233–244 (2019).
[6] A. Rodger, "UV absorbance spectroscopy of biological macromolecules," in *Encyclopedia of Biophysics*, edited by G. C. K. Roberts (Springer Heidelberg, New York, Dordrecht, London, 2013), pp. 2714–2718, ISBN: 978-3-642-16711-9.
[7] S. Majety, J. Li, X. K. Cao, R. Dahal, B. N. Pantha, J. Y. Lin, and H. X. Jiang, "Epitaxial growth and demonstration of hexagonal BN/AlGaN p-n junctions for deep ultraviolet photonics," Appl. Phys. Lett. **100**, 061121 (2012).
[8] T. Makimoto, K. Kumakura, Y. Kobayashi, T. Akasaka, and H. Yamamoto, "A vertical InGaN/GaN light-emitting diode fabricated on a flexible substrate by a mechanical transfer method using BN," Appl. Phys. Express **5**, 072102 (2012).
[9] Y. Kobayashi, K. Kumakura, T. Akasaka, and T. Makimoto, "Layered boron nitride as a release layer for mechanical transfer of GaN-based devices," Nature **484**, 223 (2012).
[10] T. T. Tran, K. Bray, M. J. Ford, M. Toth, and I. Aharonovich, "Quantum emission from hexagonal boron nitride monolayers," Nat. Nanotechnol. **11**, 37–41 (2016).
[11] R. Bourellier, S. Meuret, A. Tararan, O. Stéphan, M. Kociak, L. H. G. Tizei, and A. Zobelli, "Bright UV single photon emission at point defects in h-BN," Nano Lett. **16**, 4317–4321 (2016).

[12]For a review see B. Gil, G. Cassabois, R. Cusco, G. Fugallo, and L. Artus, "Boron nitride for excitonics, nano photonics, and quantum technologies," Nanophotonics **2020**, 20200225.
[13]K. Watanabe and T. Taniguchi, "Far-UV PL microscope for impurity domain in hexagonal-boron-nitride single crystals by high-pressure, high-temperature synthesis," npj 2D Mater. Appl. **3**, 40 (2019).
[14]R. Ishii, M. Funato, and Y. Kawakami, "Pushing the limits of deep-ultraviolet scanning near-field optical microscopy," APL Photonics **4**, 070801 (2019).
[15]S. Liu, R. He, X. Z. Du, J. Lin, H. Jiang, B. Liu, and J. H. Edgar, Cryst. Growth Des. **17**, 4932 (2017).
[16]S. Liu, R. He, L. Xue, J. Li, B. Liu, and J. H. Edgar, "Single crystal growth of millimeter-sized monoisotopic hexagonal boron nitride," Chem. Mater. **30**, 6222 (2018).
[17]J. Li, C. Elias, G. Ye, D. Evans, S. Liu, R. He, G. Cassabois, B. Gil, P. Valvin, B. Liu, and J. H. Edgar, "Single crystal growth of monoisotopic hexagonal boron nitride from a Fe-Cr flux," J. Mater. Chem. C (published online).
[18]R. Bourrellier, M. Amato, L. H. G. Tizei, C. Giorgetti, A. Gloter, M. I. Heggie, K. March, O. Stéphan, L. Reining, M. Kociak, and A. Zobelli, "Nanometric resolved luminescence in h-BN flakes: Excitons and stacking order," ACS Photonics **1**, 857 (2014).
[19]T. Pelini, C. Elias, R. Page, L. Xu, S. Liu, J. Li, J. Edgar, A. Dréau, V. Jacques, P. Valvin, B. Gil, and G. Cassabois, "Shallow and deep levels in carbon-doped hexagonal boron nitride crystals," Phys. Rev. Mater. **3**, 094001 (2019).
[20]G. Cassabois, P. Valvin, and B. Gil, "Hexagonal boron nitride is an indirect band gap semiconductor," Nat. Photonics **10**, 262 (2016).
[21]T. Q. P. Vuong, G. Cassabois, P. Valvin, V. Jacques, R. Cusco, L. Artus, and B. Gil, "Overtones of interlayer shear modes in the phonon-assisted emission spectrum of hexagonal boron nitride," Phys. Rev. B **95**, 045207 (2017).
[22]G. Cassabois, P. Valvin, and B. Gil, "Intervalley scattering in hexagonal boron nitride," Phys. Rev. B **93**, 035207 (2016).
[23]L. Schué, L. Sponza, A. Plaud, H. Bensalah, K. Watanabe, T. Takashi, F. Ducastelle, A. Loiseau, and J. Barjon, "Bright luminescence from indirect and strongly bound excitons in h-BN," Phys. Rev. Lett. **122**, 067401 (2019).
[24]C. Elias, P. Valvin, T. Pelini, A. Summerfield, C. J. Mellor, T. S. Cheng, L. Eaves, C. T. Foxon, P. H. Beton, S. V. Novikov, B. Gil, and G. Cassabois, "Direct band-gap crossover in epitaxial monolayer boron nitride," Nat. Commun. **10**, 2639 (2019).
[25]L. Schué, B. Berini, A. C. Betz, B. Plaçais, F. Ducastelle, J. Barjon, and A. Loiseau, "Dimensionality effects on the luminescence properties of hBN," Nanoscale **8**, 6986 (2016).
[26]A. Zobelli, A. Gloter, C. P. Ewels, G. Seifert, and C. Colliex, "Electron knock-on cross section of carbon and boron nitride nanotubes," Phys. Rev. B **75**, 245402 (2007).
[27]A. Zobelli, A. Gloter, C. P. Ewels, and C. Colliex, "Shaping single walled nanotubes with an electron beam," Phys. Rev. B **77**, 045410 (2008).
[28]J. Kotakoski, C. H. Jin, O. Lehtinen, K. Suenaga, and A. V. Krasheninnikov, "Electron knock-on damage in hexagonal boron nitride monolayers," Phys. Rev. B **82**, 113404 (2010).
[29]J. C. Meyer, A. Chuvilin, G. Algara-Siller, J. Biskupek, and U. Kaiser, "Selective sputtering and atomic resolution imaging of atomically thin boron nitride membranes," Nano Lett. **9**, 2683 (2009).
[30]C. Jin, F. Lin, K. Suenaga, and S. Iijima, "Fabrication of a freestanding boron nitride single layer and its defect assignments," Phys. Rev. Lett. **102**, 195505 (2009).
[31]O. Mouhoub, R. Martinez-Gordillo, J. Nelayah, G. Wang, J.-H. Park, K. K. Kim, Y. H. Lee, C. Bichara, A. Loiseau, C. Ricolleau, H. Amara, and D. Alloyeau, "Quantitative insights into the growth mechanisms of nanopores in hexagonal boron nitrile," Phys. Rev. Mater. **4**, 014005 (2020).
[32]A. Zobelli, S. Y. Woo, A. Tararan, L. H. G. Tizei, N. Brun, X. Li, O. Stéphan, M. Kociak, and M. Tencé, "Spatial and spectral dynamics in STEM hyperspectral imaging using random scan patterns," Ultramicroscopy **212**, 112912 (2020).
[33]L. F. Zagonel, S. Mazzucco, M. Tencé, K. March, R. Bernard, B. Laslier, G. Jacopin, M. Tchernycheva, L. Rigutti, F. H. Julien, R. Songmuang, and M. Kociak, Nano Lett. **11**(2), 568–573 (2011).
[34]S. Meuret, L. H. G. Tizei, T. Auzelle, R. Songmuang, B. Daudin, B. Gayral, and M. Kociak, "Lifetime measurements well below the optical diffraction limit," ACS Photonics **3**(7), 1157–1163 (2016).
[35]See for instance *Advances in Imaging and Electron Physics*, edited by P. W. Hawkes and M. Hÿtch (Academic Press, 2019), Vol. 209, ISBN: 9780128171776.